Journal of Chromatography A, 1322 (2013) 81–89

Contents lists available at ScienceDirect

Journal of Chromatography A

journal homepage: www.elsevier.com/locate/chroma

Inverse gas chromatography applied in the surface properties evaluation of mesocellular silica foams modified by sized nickel nanoparticles

Linping Qian[a,b,*], Ximeng Lv[a], Yu Ren[a], Haitao Wang[b,**], Guoping Chen[c], Yuanli Wang[a], Jianzhong Shen[a]

[a] Department of Chemistry, Shanghai Key Laboratory of Molecular Catalysis and Innovative Materials, Fudan University, Shanghai, 200433, PR China
[b] State Key Laboratory of Molecular Engineering of Polymers, Department of Macromolecular Science, Fudan University, Shanghai, 200433, PR China
[c] State Key Laboratory of ASIC & System and School of Microelectronics, Fudan University, Shanghai, 200433, PR China

ARTICLE INFO

Article history:
Received 28 September 2013
Accepted 30 October 2013
Available online 6 November 2013

Keywords:
Inverse gas chromatography
MCF
Nickel
Adsorption
Surface properties

ABSTRACT

The mesocellular silica foams (MCF) modified by different sized Ni nanoparticles (≤27.4 nm) were prepared through the wetness impregnation of low metal content (0.5–2.0 wt%). The technology of inverse gas chromatography (IGC) was used to evaluate the size effect of Ni nanoparticles on the surface property of Ni/MCF and the probes of four *n*-alkanes (C_6–C_9), cyclohexane, benzene, toluene, trichloroethylene, and tetrachloroethylene were tested in the 463.2–493.2 K temperature range. High free energy of adsorption and enthalpy of adsorption for the aromatic hydrocarbons were found over 1.0 wt% Ni/MCF with small nanoparticles of ca. 5 nm. The dispersive interaction parameter γ_S^D, and specific interaction parameter I^{sp} increase with Ni nanoparticle size decreasing over Ni/MCF. The results indicate that Ni species highly dispersed on MCF support significantly promote the surface property of the specific interaction with the aromatic structure.

1. Introduction

During the past decades, nickel based catalysts have been intensively studied and show promising catalytic performance especially in hydrogenation of aromatic hydrocarbons [1–3]. For example, Al_2O_3 supported Ni catalysts showed good catalytic performance in hydrogenation of benzene [1] and small Ni particle (≤4 nm) loaded on the support promotes turnover frequency (TOF) of benzene significantly [2]. Ni supported on ZrO_2 achieved high activity and stability in hydrogenation of the aromatic ring of phenol [3]. Mesocellular silica foam (MCF) is a newly reported aerogel-like mesoporous silica material [4]. Besides the thermal stability similar to other silica materials such as MCM-41 or SBA-15, MCF has the advantage of better diffusion of reactants for its 3D continuous mesopore system and interconnected windows (Fig. 1) [5]. Although there is much interest on the catalytic property of metal containing catalysts [1–3] and MCF [6], there are no detailed studies on the surface properties of MCF modified by different sized nickel particles.

It is well known that the solid surfaces can be studied by adsorption of gases and vapors through static or dynamic methods, e.g. inverse gas chromatography (IGC). IGC is performed by injecting certain probes into a column containing the target solid for the surface characterization. The retention time or the retention volume of the adsorbate, measured near zero surface coverage, allows not only the determination of the interactions between the adsorbates and the adsorbents but also the characterization of the surface properties of the target materials [7]. IGC has been successfully employed in studying thermodynamics parameters, surface energy, reaction kinetics, textural parameters and acid/base character of many solid materials [7–18] including the metal loading catalysts such as Rh/H-Beta [12], NaX, CaA [13], γ-Al_2O_3 supported noble metals [14,18], etc. For the alkali and alkaline metal modifying, Milonjic used IGC to study the surface properties of Li, Na, K, Cs, Ba and Mg loaded on the silica beads, and found that the adsorption free energy of alkanes decreases and the homogeneity of the modified silica surface improves through the retention time determination and chromatographic peaks analysis [17]. For the transitional metal loading, Pt, Rh, Ru and Pd were disclosed to modify the surface properties differently by IGC. Ordonez et al. studied the surface adsorption properties of γ-Al_2O_3 supported Pt,

* Corresponding author at: Department of Chemistry, Shanghai Key Laboratory of Molecular Catalysis and Innovative Materials, Fudan University, Shanghai, 200433, PR China. Tel.: +86 21 65642796; fax: +86 21 65641740.
** Corresponding author at: State Key Laboratory of Molecular Engineering of Polymers, Department of Macromolecular Science, Fudan University, Shanghai, 200433, PR China. Tel.: +86 21 65642392; fax: +86 21 65640293.
E-mail addresses: lpqian@fudan.edu.cn (L. Qian), wanght@fudan.edu.cn (H. Wang).

0021-9673/$ – see front matter © 2013 Elsevier B.V. All rights reserved.
http://dx.doi.org/10.1016/j.chroma.2013.10.091

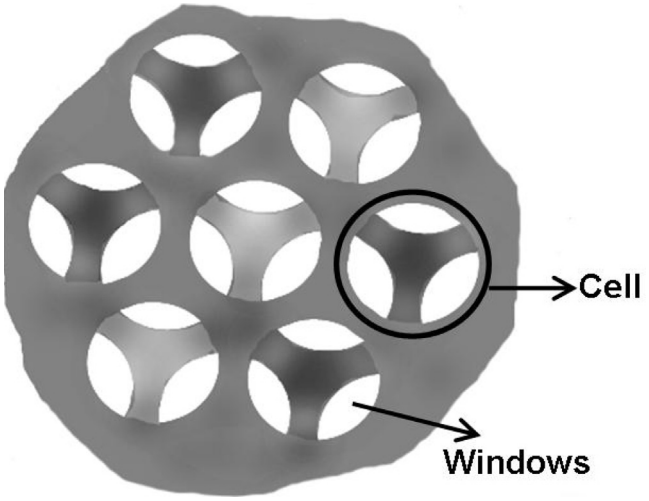

Fig. 1. Structure of MCF [4,5].

Rh and Ru catalysts and found that the catalyst treatment affects the adsorption nature greatly. Hydrogen-treated Rh and Ru catalysts present higher specific interaction with aromatic structure, while oxygen-treated Pt one possesses the highest [14]. They also investigated γ-Al_2O_3 modified by Pd catalysts and found that Pd loading cannot enhance the specific interaction with aromatic structure but with non-aromatics one [18]. In our previous work, the surface properties of Rh/H-Beta catalyst were characterized by IGC and its special interaction with benzene was found [12]. Based on this finding, Rh/H-Beta was filled in polyvinyl chloride membranes and showed very good separation selectivity in pervaporation of benzene/cyclohexane mixtures [19]. Another sophisticated IGC technique is reversed-flow GC (or time-resolved GC), which can be used in the examination of catalytic reaction rate constants, time adsorption energies, adsorption isotherm parameters, adsorption rates with lateral molecular interactions, surface diffusion coefficients etc. [20–22]. Katsanos et al. achieved in surface energy evaluation of Pt–Rh supported on SiO_2 catalysts by this IGC technique and determined that the catalyst containing the preferable weight ratio of Pt:Rh = 3:1 possesses high separation properties [20].

In this present work, different sized Ni particles were loaded on MCF through incipient wetness impregnation of low metal content. The surface properties of MCF and Ni/MCF were investigated by IGC. The free energy of adsorption, the heat of adsorption, the surface free energy, as well as their specific and dispersive components are also presented. The chromatographic data could provide information on the interaction between the adsorbed molecules and the catalysts, and disclose the effect of the different sized metal particle on the surface properties of the catalysts, which can help to design the related hybrid membranes, adsorbents, catalysts etc.

2. Experimental

2.1. Catalyst preparation

MCF is composed of uniformly sized, large spherical cells that are interconnected by uniformly windows to a continuous 3-D pore system (Fig. 1). The samples were prepared according to the literatures reported [4,5]. Pluronic P123 triblock copolymer ($EO_{20}PO_{70}EO_{20}$, average Mn of 5800, Aldrich) was dissolved in aqueous HCl solution (2 mol dm^{-3}) under stirring at ambient temperature and 1,3,5-trimethylbenzene (TMB, 99%, Aldrich) was added. After heated 1 h at 313 K, tetraethyl orthosilicate (TEOS, analytical reagent grade, China Sinopharm Chemical Reagent Co. Ltd.) was added. After stirring for 20 h, the cloudy mixture with a molar ratio of $EO_{20}PO_{70}EO_{20}$:TEOS:HCl:TMB = 4:210:1200:170 was moved into a Teflon-lined stainless autoclave and kept at 368 K for 24 h. The filtered precipitate was dried and calcined at 773 K for 8 h in air. According to the literature reported by Poncelet [2], nickel particle size on the support can be adjusted by simply changing metal loading content. Thus, MCF supported with different sized Ni particle was prepared by impregnating the support with $Ni(NO_3)_3{\cdot}6H_2O$ solution (0.20 mol dm^{-3}) to yield a nominal metal content. After drying under an infrared lamp, the catalyst was calcined in air at 573 K for 30 min and then reduced in H_2/Ar (5% H_2) at 773 K for 60 min.

2.2. Characterization of the catalysts

Small-angle X-ray scattering (SAXS) experiments were performed on a Bruker NanoSTAR U SAXS system equipped with high-resolution pinhole chamber using Cu-K_α radiation (λ = 0.15418 nm). Wide-angle X-ray diffraction (XRD) patterns were recorded using a Rigaku D/MAX-IIA diffractometer with Cu-K_α radiation (λ = 0.15418 nm). N_2 adsorption/desorption data were obtained using a Micromeritics Tristar-3000 (Quantachrome) apparatus at 77 K. The samples were pretreated at 573 K under vacuum for 3 h before N_2 adsorption. The surface area was calculated by the BET method, and the pore diameter distribution was evaluated by the BJH model. Transmission electron microscopy (TEM) measurements were performed on a JEOL JEM-2011 transmission electron microscopy. Prior to the measurement, the samples were mounted on carbon-coated copper grid by drying a droplet of a suspension of the ground sample in ethanol on the grid.

2.3. IGC apparatus and procedure

IGC experiments were carried out with a GC112A gas chromatography (Shanghai Precision and Scientific Instrument Co. Ltd., China) equipped with a flame ionization detector. Retention time was recorded on a workstation (Shanghai Wuhao Information Technology Co. Ltd., China). High purity nitrogen (≥99.999%, China Sinopharm Chemical Reagent Co. Ltd.) was used as the carrier gas with a flow rate of ca. 28 mL min^{-1}. The flow rate of the carrier gas was measured by a soap bubble flowmeter at the detector outlet and was corrected using James-Martin factor for pressure drop and temperature change in the column (Eq. (1)).

$$V_N = Fj(t_R - t_d)\left(\frac{p_o - p_w}{p_o}\right)\left(\frac{T}{T_{meter}}\right) \quad (1)$$

where t_R is the retention time, t_d, the dead time, p_o, the outlet column pressure, p_w, the vapor pressure of water at the flowmeter temperature, T_{meter}, the ambient temperature, and j, the James-Martin compressibility factor defined as:

$$j = \frac{3}{2}\left[\frac{(p_i/p_o)^2 - 1}{(p_i/p_o)^3 - 1}\right] \quad (2)$$

where p_i, the inlet pressure.

The probes used were *n*-hexane, *n*-heptane, *n*-octane, *n*-nonane, cyclohexane, trichloroethylene, tetrachloroethylene, benzene and toluene (analytical reagent grade, Shanghai Chemical Reagents Company). A stainless steel column (30 cm long, 2 mm i.d.) was packed with 0.2 g of 60–80 mesh catalyst powders. The two ends of the column were plugged with silane-treated glass wool. Before the adsorption test of the probes, the column was stabilized on the GC system at 503.2 K overnight under a nitrogen flow of about 28 mL min^{-1}. All the tests were carried out in the temperature range from 463.2 to 493.2 K. In order to meet the requirement of adsorption at infinite dilution, the probes were injected into the column with the injected vapor volume lower than 0.1 μL. Thus, the

solute–solute interaction can be neglected and the retention on the catalyst surface is only up to catalyst–probe interaction. Furthermore, the isotherm data obtained in the injected probe from 0.05 μL to 0.5 μL using the peak maxima method [16,18] falls into a straight line with regression coefficients $R^2 \geq 0.990$, indicating the experiments obeyed the Henry' law in zero coverage region and absence of interactions between solute probes. For each measurement, methane was used to measure the dead volume t_d, which was employed in the retention-time t_R correction for the absence of the dead volume in the test column. At least three replicative determinations were used in averaging the net retention volume (V_N). The typical chromatograms obtained (Fig. 1S Supplementary data) are sharp and characterized by a good symmetry. The test results demonstrate that IGC test can be conducted on Ni/MCF with few interference of strong heterogeneous structure [12,16–18].

Supplementary material related to this article can be found, in the online version, at http://dx.doi.org/10.1016/j.chroma.2013.10.091.

2.4. Models and calculations

2.4.1. Standard free energy of adsorption

At infinite dilution, the standard free energy of adsorption, ΔG_{ads} (J mol^{-1}), is given by the following equation [7,17,23–25]:

$$\Delta G_{ads} = -RT \ln \frac{V_N p_{s,g}}{\pi_s m S} \quad (3)$$

where R is the gas constant, m is the mass of the catalyst in the column, S is the specific surface area of the catalysts determined by BET methods through N_2 adsorption analysis, $p_{s,g}$ is reference pressure having a value of 1 atm (101,325 N/m^2) and π_s is the vapor pressure at equilibrium with the standard adsorption state, 0.338 mN/m (the De Boer standard state) [24]. According to the definition of adsorption free energy, the investigated catalysts with somewhat different surface area can be compared with the unified scale [12,13,16].

2.4.2. Enthalpy of adsorption

The heat of adsorption ΔH_{ads} can be calculated from Gibbs–Helmotz equation:

$$\Delta H_{ads} = -R \frac{\partial(\ln V_N)}{\partial(1/T)} \quad (4)$$

2.4.3. Standard surface free energy: specific and dispersive components

The standard free energy of adsorption takes into account the standard free energy of adsorption of polar solutes on solid surfaces, namely, the dispersive contribution, ΔG^d_{ads}, and the specific contribution, ΔG^s_{ads}. For n-alkanes, $\Delta G_{ads} = \Delta G^d_{ads}$ and the increment of adsorption energy corresponding to the free energy of adsorption of a methylene group (ΔG_{CH_2}) is defined as the energy difference for the adsorption of two successive alkanes having n and $n+1$ atoms of carbon (octane/nonane, nonane/decane, etc.). According to Dorris and Gray [25], dispersive component of the surface energy (γ^D_S), intrinsic and unspecific for all molecules, can be calculated by Eq. (5) by use of experimentally determined ΔG_{CH_2}:

$$\gamma^D_S = \frac{1}{4} \frac{\Delta G^2_{CH_2}}{\gamma_{CH_2} N^2 a^2_{CH_2}} \quad (5)$$

where N is the Avogadro number, a_{CH_2} is the cross sectional area occupied by a methylene group (0.06 nm^2), and γ_{CH_2} (mJ m^{-2}) is the surface tension of a solid consisting of —CH_2— groups. In this test, the dispersive component of the surface energy was determined by non-polar probes with successive —CH_2— group such as hexane, heptane, octane and nonane. The specific component of the surface free energy is closely related with the parameter of specific interaction of polar solutes (I^{sp}) with the catalyst. This parameter represents the sum of all non-dispersive interactions, which involves the surface properties in terms of electron, potential and acid–base interactions. I^{sp} may be determined from the difference of free energy of adsorption, $\Delta(\Delta G)$, between a polar solute and the real or hypothetical n-alkane with the same surface area [23] or boiling point, T_b [26], as shown in the following equation:

$$I^{sp} = \frac{\Delta(\Delta G)}{N a_p} \quad (6)$$

where a_p of the polar probe surface area is used in this work. Although this treatment is empirical, the specific interaction between the test solid and the probe molecule can be compared with a unified scale. For the non-dispersive surface energy, electrical and polar interaction other than the London type was investigated by aromatic ring of benzene and toluene, comparative cyclic structure of cyclohexane and the similar compounds with different polarity such as trichloroethylene and tetrachloroethylene.

Table 1
Characteristics of MCF and Ni/MCF samples.

Samples[a]	S_{BET} (m^2/g)	V_t [b] (cm^3/g)	Pore size[c] adsorption (nm)	Pore size[c] desorption (nm)
MCF	619	1.6	22.1	7.6
0.5 wt% Ni/MCF	534	1.0	21.1	5.4
1.0 wt% Ni/MCF	531	1.0	20.7	5.3
2.0 wt% Ni/MCF	502	1.0	20.3	5.3

[a] S_{BET}, BET surface area deduced from N_2 isotherms in the relative pressure range 0.05–0.30.
[b] V_t, total adsorption pore volume at relative pressure 0.99.
[c] Pore size of adsorption and desorption determined according to the BJH method.

3. Results and discussion

3.1. Catalyst characterization

SAXS data for MCF and Ni/MCF catalysts are shown in Fig. 2(a). All samples exhibit one strong primary peak at $2\theta = 0.39^\circ$ and two higher-order peaks around $2\theta = 0.68^\circ$ and 0.93° with exponentially decreasing intensities. The occurrence of the higher-order peaks is an indication of the narrow size distribution of the spherical cells. The SAXS results show that the structure order of the materials is mainly maintained for MCF after Ni introduction [4–6]. Wide angle XRD patterns (Fig. 2(b)) of MCF and Ni/MCF catalysts shows a broad peak around 15–30° (2θ) which was ascribed to the amorphous silica composition. Another peak at 44.4° was found over Ni/MCF with Ni loading not less than 1.0 wt%, attributing to the (1 1 1) diffraction of nickel metal crystals [27].

Fig. 3 shows the N_2 sorption isotherms of Ni/MCF catalysts. The isotherms are of type IV and show steep H1 type hysteresis at high-relative pressures (Fig. 3(a)), which not only exhibits the capillary condensation and evaporation of the typical mesoporous materials but also indicates the large pore sizes with narrow size distributions (Fig. 3(b)) [5,28,29]. The BET specific surface areas, pore sizes and pore volumes of all samples are presented in Table 1. The BET surface areas are between 500 and 650 m^2/g for all samples, which coincide with the reported values [4–6]. The BET surface areas, pore volumes and pore sizes decrease with introduction of Ni species. This phenomenon could be explained by the blockage of MCF windows with the introduction of Ni species.

TEM images (Fig. 4) of Ni/MCF reveal a disordered array of silica struts comprising uniformly sized spherical cells (20–40 nm) interconnected by windows with a narrow size distribution, which is

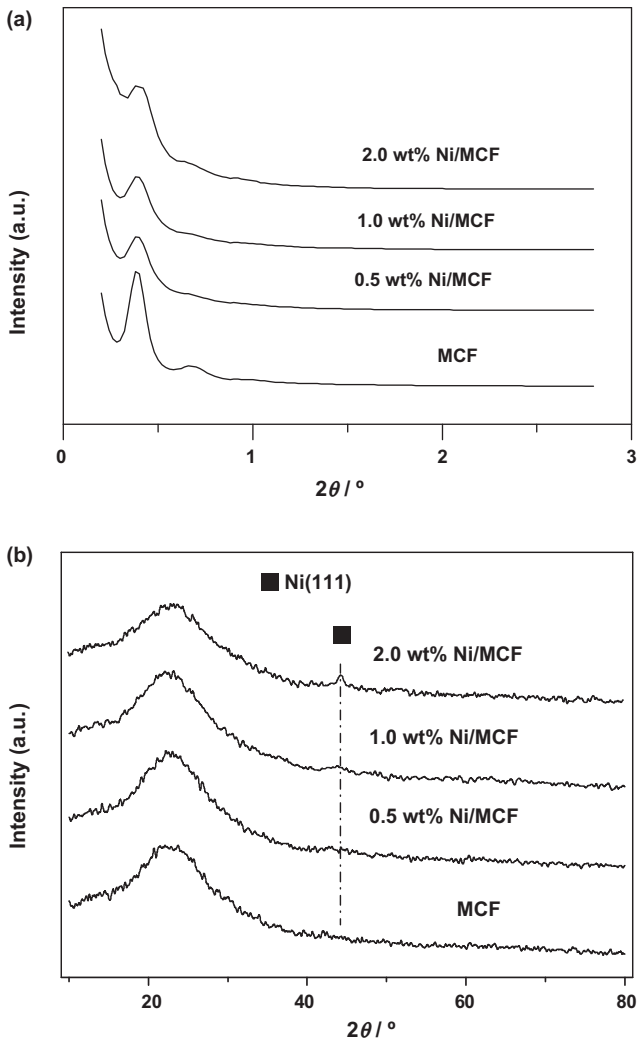

Fig. 2. Small-angle X-ray scattering patterns (a) and wide-angle X-ray diffraction patterns (b) of MCF and Ni/MCF samples.

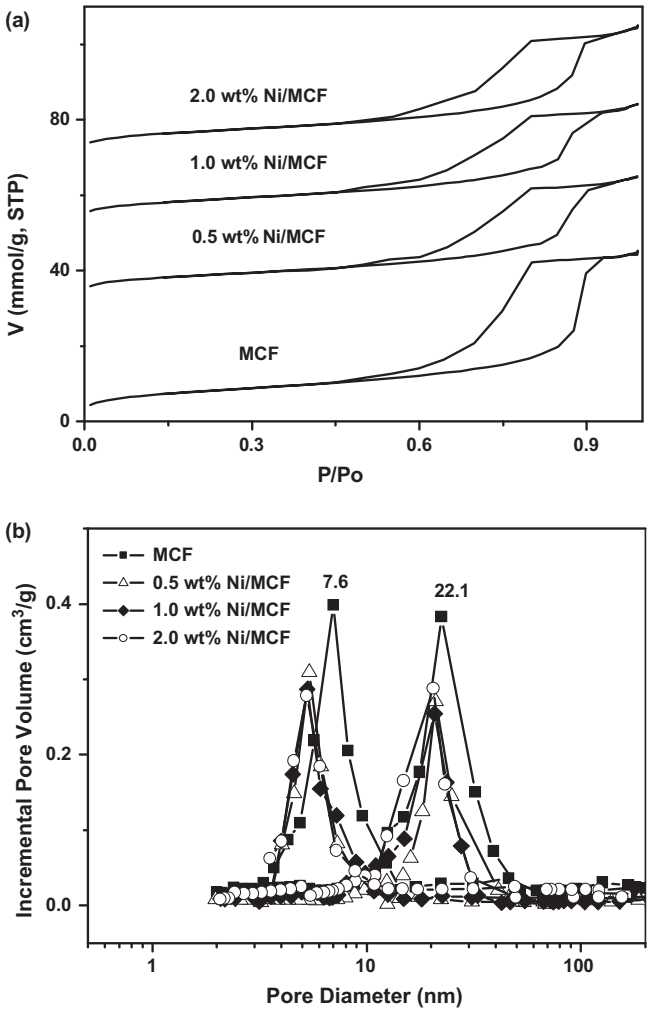

Fig. 3. Nitrogen sorption isotherms (a) and pore size distribution of adsorption and desorption branches according to the BJH method (b) for MCF and Ni/MCF samples.

the characteristic of the MCF materials [4,5]. The strut-like structure observed by TEM resembles that of aerogels [4]. It is noticeably observed that the large nickel nanoparticles form over MCF with Ni loading content ≥1.0 wt%. From the size analysis of 100 nanoparticles based on TEM, the average particle size is ca. 5.0 nm over 1.0 wt% Ni/MCF (particle size distribution: 1.4–9.5 nm) in Fig. 4(c), and ca. 14.4 nm over 2.0 wt% Ni/MCF (particle size distribution: 6.2–27.4 nm) in Fig. 4(d). From the above study, it indicates that the continuous 3D pore structure of the MCF is maintained after Ni introduction through wetness impregnation method. With more Ni impregnation (≥1.0 wt%), Ni species begins to aggregate and forms larger metal particles.

3.2. Inverse gas chromatography

3.2.1. Influence of the carrier gas flow rate on measurements

Before the IGC test on Ni/MCF and MCF, it is necessary to separate the probe adsorption on the external surface from the probe diffusion. It is well understood that the net retention volume should be independent of the flow rate if the measurement is not limited by diffusion effects. Similar results were reported to separate the surface adsorption contribution through adjusting the carrier gas flow rates [16,30,31]. The variation of the specific retention volume of *n*-alkanes is shown in Fig. 5 as a function of the carrier gas flow rate with Ni/MCF and MCF as stationary phases at 473.2 K. It can be observed that the retention data were independent of the carrier gas flow rate over MCF and Ni/MCF when the carrier gas flow rate is above 20 mL min^{-1}, indicating the measurements under such flow rates are not limited by diffusion effects. According to Fig. 5, the nitrogen flow rate of 28 mL min^{-1} was chosen for the test study.

3.2.2. Free energy of adsorption

Based on Eq. (3), the standard free energy of adsorption obtained is shown in Table 2. The adsorption energy decreases with the temperature increasing, following the van't Hoff equation. For the aromatic hydrocarbons, its standard free energy is higher than cyclic and aliphatic hydrocarbons with the same carbon number. This could be attributed to two main interactions. One is between the weak acid sites of the hydroxyls on the silica [32,33] and the aromatic compounds containing π electrons (significant Lewis bases)[13,16,18], the other is between *d* orbits of Ni and π electrons of aromatic probes [12]. For the chlorinated compounds, the polar molecule of trichloroethylene shows an increase of the standard free energy due to the existing polar bridge-oxygen atom of Si—O—Si for the samples. The obtained value of the adsorption free energy on MCF is higher than that of mesoporous materials e.g. γ-Al_2O_3 [34], KIT-6-1223 K [16] and SiO_2—H [17] but similar to micro-mesoporous materials such as KIT-6-773 K [16]. After Ni loading, the adsorption free energy increases about 1 kJ mol^{-1} for the aromatics, which could be attributed to the extra interaction

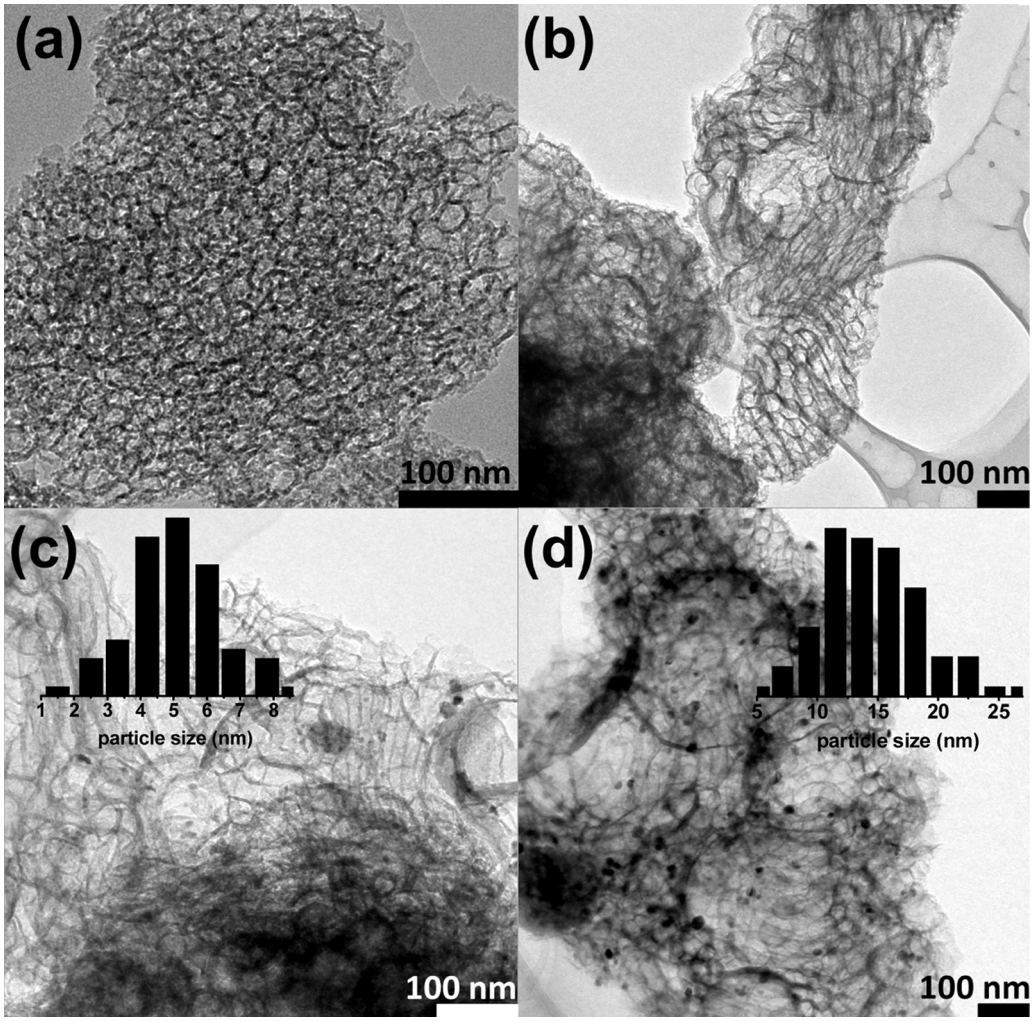

Fig. 4. TEM images of Ni/MCF samples: (a) MCF; (b) 0.5 wt% Ni/MCF; (c) 1.0 wt% Ni/MCF; (d) 2.0 wt% Ni/MCF.

between the transitional metal of Ni and the aromatic compounds containing π electrons [12]. Most negative for aromatics adsorption is found on 1.0 wt% Ni/MCF. This indicates the stronger interaction of the aromatic compounds occurs on MCF not loaded with more Ni species but with metal forming structure of smaller particle. However, considering the error in the free adsorption energy in Table 2, this promotion effect cannot be distinguished clearly for 1.0 wt% Ni/MCF with 0.5 wt% Ni/MCF in the test.

3.2.3. Enthalpy of adsorption

Enthalpies of adsorption ΔH_{ads} can be obtained from the slope of the plot of $R \ln V_N$ versus $1/T$ (Fig. 6) based on Eq. (4), and the results are summarized in Table 3. The dependence of adsorption enthalpies for *n*-alkanes (C_6–C_9) as a function of the adsorbate size, on both MCF and 2.0 wt% Ni/MCF, shows a straight line in Fig. 6. The adsorption enthalpies of *n*-alkanes increases with the carbon number increment, which is ascribed to the increasing condensation heat of *n*-alkanes onto the solid surface and the stronger physico-chemical interactions between probes and adsorbents due to the chain growth [12,16,18]. Due to the error in fitness analysis (Fig. 6), the adsorption enthalpy of alkanes on MCF is not discriminated from that on 2.0 wt% Ni/MCF. For the chlorinated compounds on Ni/MCF samples in Table 3, trichloroethylene exhibits higher adsorption enthalpy than tetrachloroethylene, indicating the maintenance of the polar interaction between the adsorbate and the adsorbent after Ni introduction. Compared with MCF, benzene shows more negative ΔH_{ads} over Ni/MCF than cyclic hydrocarbons and aliphatic hydrocarbons with the same carbon number, i.e. cyclohexane and hexane. This increment is similar to free energy of adsorption and could also be attributed to the special interaction between Ni species and benzene. The most negative for benzene adsorption enthalpy occurs on 1.0 wt% Ni/MCF with particle size of ca. 5 nm. However, in determining the adsorption enthalpies through linear fitness of $R \ln V_N$ versus $1/T$, the error for benzene and toluene is great (Table 3), which cannot cause the significant difference from the varied content Ni (≤2.0 wt%) loaded on MCF.

3.2.4. Standard surface free energy

Dispersive component of surface free energy, ΔG_{CH_2} may be determined from a plot of ΔG_{ads} versus the number of carbon atoms of the *n*-alkanes adsorbed on the solid surface. Then, the γ_S^D value can be calculated through Eq. (5). The dispersive interaction on MCF and Ni/MCF samples at different temperature is shown in Fig. 7, in which the γ_S^D value decreases at elevated temperature due to the entropic contribution ($-T(\Delta S_{CH_2})$) [12,16–18,34]. Noticeably the dispersive component of surface free energy over the temperature range examined is enhanced for MCF after Ni modification, which could be attributed to the extra interaction between Ni nanoparticles and the *n*-alkanes. The highest interaction occurs on 0.5 wt% Ni/MCF with small metal particle which cannot be observed by XRD and TEM. Similar phenomena have been observed on Rh/H-Beta catalysts that 0.5 wt% Rh/H-Beta shows higher dispersive

Table 2
Standard free energy of adsorption, $-\Delta G_{ads}$ (kJ mol^{-1}) for the probes on catalysts.

Adsorbent/probe	Temperature (K)			
	463.2	473.2	483.2	493.2
MCF				
Hexane	9.58 ± 0.06	9.01 ± 0.08	8.35 ± 0.09	7.92 ± 0.09
Heptane	13.20 ± 0.04	12.34 ± 0.04	11.64 ± 0.05	11.03 ± 0.08
Octane	16.38 ± 0.12	15.57 ± 0.12	14.81 ± 0.12	14.19 ± 0.05
Nonane	19.69 ± 0.15	18.77 ± 0.08	18.00 ± 0.03	17.40 ± 0.02
Cyclohexane	10.38 ± 0.05	9.65 ± 0.06	9.26 ± 0.04	8.53 ± 0.10
Trichloroethylene	11.23 ± 0.03	10.59 ± 0.06	10.18 ± 0.07	9.71 ± 0.07
Tetrachloroethylene	10.43 ± 0.05	9.71 ± 0.07	9.12 ± 0.05	8.76 ± 0.06
Benzene	12.10 ± 0.03	11.39 ± 0.04	10.71 ± 0.05	10.30 ± 0.07
Toluene	15.89 ± 0.12	15.16 ± 0.03	14.47 ± 0.14	14.02 ± 0.03
0.5 wt% Ni/MCF				
Hexane	8.81 ± 0.15	8.30 ± 0.16	7.69 ± 0.09	7.12 ± 0.09
Heptane	12.41 ± 0.13	11.81 ± 0.15	11.19 ± 0.15	10.69 ± 0.10
Octane	15.89 ± 0.12	15.20 ± 0.13	14.78 ± 0.13	13.72 ± 0.14
Nonane	19.50 ± 0.12	18.79 ± 0.12	18.03 ± 0.03	17.48 ± 0.06
Cyclohexane	9.87 ± 0.09	9.46 ± 0.07	8.83 ± 0.08	8.22 ± 0.09
Trichloroethylene	12.28 ± 0.09	11.85 ± 0.04	11.32 ± 0.04	10.82 ± 0.06
Tetrachloroethylene	10.11 ± 0.07	9.70 ± 0.04	9.18 ± 0.08	8.51 ± 0.09
Benzene	12.89 ± 0.16	12.25 ± 0.07	11.64 ± 0.09	10.97 ± 0.06
Toluene	16.77 ± 0.13	16.11 ± 0.14	15.51 ± 0.12	14.80 ± 0.04
1.0 wt% Ni/MCF				
Hexane	9.08 ± 0.09	8.35 ± 0.07	7.80 ± 0.10	7.35 ± 0.15
Heptane	12.55 ± 0.04	11.78 ± 0.13	11.09 ± 0.05	10.49 ± 0.14
Octane	15.88 ± 0.13	14.97 ± 0.12	14.30 ± 0.12	13.81 ± 0.12
Nonane	19.34 ± 0.11	18.48 ± 0.12	17.65 ± 0.04	17.07 ± 0.13
Cyclohexane	9.88 ± 0.06	9.15 ± 0.09	8.52 ± 0.05	8.03 ± 0.09
Trichloroethylene	11.94 ± 0.07	11.31 ± 0.03	10.66 ± 0.02	10.02 ± 0.09
Tetrachloroethylene	9.85 ± 0.06	9.22 ± 0.09	8.52 ± 0.05	7.88 ± 0.08
Benzene	13.24 ± 0.11	12.49 ± 0.13	11.68 ± 0.03	10.98 ± 0.07
Toluene	17.12 ± 0.13	16.30 ± 0.10	15.55 ± 0.04	14.94 ± 0.02
2.0 wt% Ni/MCF				
Hexane	10.54 ± 0.06	9.78 ± 0.13	9.19 ± 0.05	8.71 ± 0.03
Heptane	14.11 ± 0.04	12.86 ± 0.05	12.46 ± 0.07	11.68 ± 0.03
Octane	17.54 ± 0.12	16.50 ± 0.13	15.84 ± 0.12	15.08 ± 0.13
Nonane	20.75 ± 0.12	19.67 ± 0.13	19.03 ± 0.12	18.29 ± 0.04
Cyclohexane	11.49 ± 0.04	10.53 ± 0.06	9.77 ± 0.04	9.22 ± 0.04
Trichloroethylene	12.23 ± 0.05	11.48 ± 0.06	10.75 ± 0.07	10.20 ± 0.04
Tetrachloroethylene	11.18 ± 0.04	10.47 ± 0.06	9.77 ± 0.05	9.12 ± 0.05
Benzene	12.88 ± 0.12	12.15 ± 0.04	11.40 ± 0.07	10.73 ± 0.08
Toluene	16.78 ± 0.12	15.85 ± 0.03	15.26 ± 0.05	14.56 ± 0.04

Table 3
Adsorption enthalpies $-\Delta H_{ads}$ (kJ mol^{-1}) on MCF and Ni/MCF samples.

Probes	MCF	0.5 wt% Ni/MCF	1.0 wt% Ni/MCF	2.0 wt% Ni/MCF
Hexane	35.8 ± 1.9 (0.996)	35.1 ± 1.3 (0.998)	35.7 ± 2.0 (0.996)	38.8 ± 2.7 (0.994)
Heptane	46.8 ± 1.6 (0.997)	39.3 ± 1.1 (0.999)	44.1 ± 1.2 (0.999)	49.7 ± 3.9 (0.976)
Octane	50.3 ± 1.3 (0.998)	47.9 ± 3.2 (0.986)	47.9 ± 2.6 (0.991)	54.7 ± 2.3 (0.995)
Nonane	55.2 ± 1.9 (0.996)	51.1 ± 1.7 (0.998)	55.5 ± 1.9 (0.996)	57.9 ± 2.5 (0.994)
Cyclohexane	37.8 ± 2.8 (0.992)	35.7 ± 1.8 (0.996)	38.6 ± 2.1 (0.995)	43.0 ± 1.0 (0.999)
Trichloroethylene	36.5 ± 1.9 (0.996)	35.1 ± 2.7 (0.992)	41.6 ± 2.3 (0.994)	43.8 ± 1.8 (0.996)
Tetrachloroethylene	35.4 ± 3.0 (0.989)	34.7 ± 3.8 (0.979)	40.3 ± 2.5 (0.992)	42.7 ± 1.7 (0.996)
Benzene	40.2 ± 2.7 (0.993)	42.3 ± 1.2 (0.999)	48.4 ± 2.2 (0.996)	46.1 ± 1.1 (0.999)
Toluene	45.1 ± 2.5 (0.995)	47.0 ± 3.4 (0.985)	50.8 ± 1.8 (0.998)	50.3 ± 2.0 (0.996)

Regression coefficients (R^2) are given in parentheses.

interaction than 1.0 wt% Rh/H-Beta and 2.0 wt% Rh/H-Beta [12]. The main reason is that the small metal nanoparticle with high dispersion interacts strongly with alkanes due to the occurrence of the coordinately unsaturated metal surface atoms [35]. With more Ni loading, the metal species favor to aggregate and form larger nanoparticles, which leads to the reduction of the coordinately unsaturated metal sites. Thus, the dispersive interaction promotion over 1.0 wt% Ni/MCF and 2.0 wt% Ni/MCF is lower than that of 0.5 wt% Ni/MCF.

As mentioned previously, the specific interaction parameter, I^{sp}, can be evaluated from the linear correlation between the probe surface area, a_p, and the adsorption free energy, ΔG_{ads}, for *n*-alkanes (Eq. (6)) (Fig. 8). The $\Delta(\Delta G)$ value is the difference of adsorption free energy between the polar molecular and *n*-alkane with same surface area. Table 4 shows the values of the specific interaction parameters at the temperature range of 463.2–493.2 K for MCF and Ni/MCF. The strong polar probe of tricholoroethylene shows higher values of I^{sp} than tetracholoroethylene, which is attributed to polar bridge oxygen atom on Si—O—Si framework surface. It is noticeable that the aromatics such as benzene shows higher values of I^{sp} than cyclohexane for MCF and Ni/MCF. This behavior is related to two main factors as the above presented. One is the acid sites of hydroxyl group which have strong interaction with aromatics containing π electrons (significant Lewis base) [13,16,18], and the

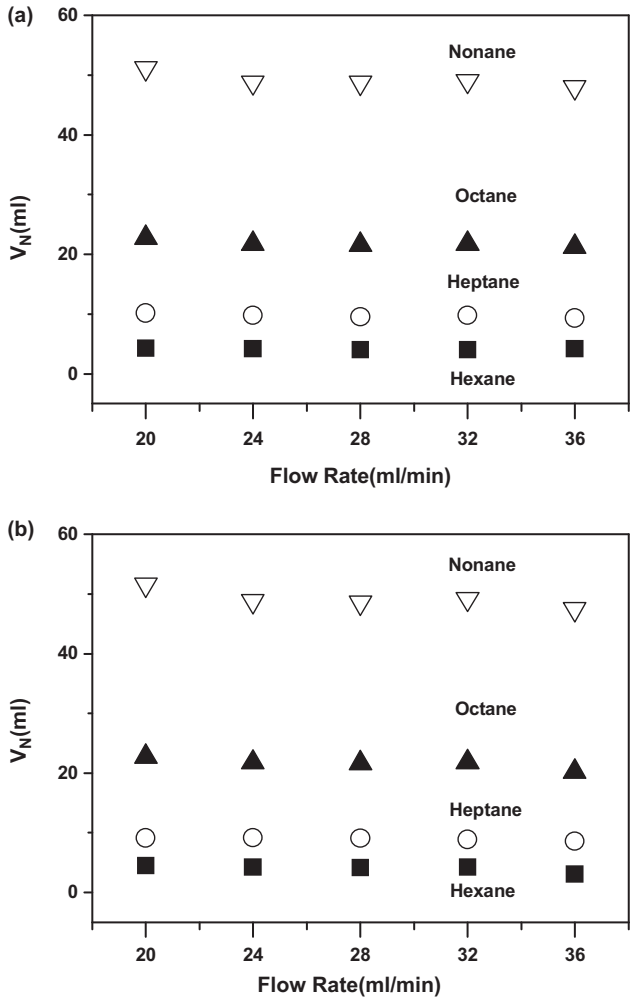

Fig. 5. Effect of carrier gas flow rate on the retention volume at 473.2 K for hexane (■), heptane (○), octane (▲), nonane (▽) over MCF (a) and 2.0 wt% Ni/MCF (b).

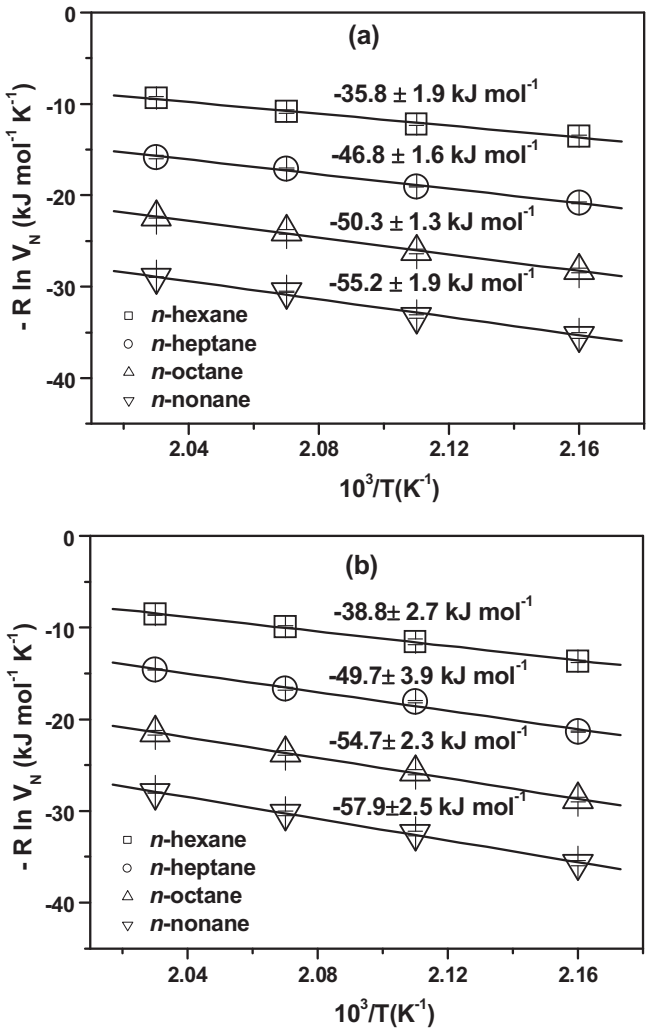

Fig. 6. Adsorption enthalpies (ΔH_{ads}) of n-alkanes on MCF (a) and 2.0 wt% Ni/MCF (b).

Table 4
I^{sp} (mJ/m^2) values determined on MCF and Ni/MCF samples.

Adsorbent/probe	Temperature (K)			
	463.2	473.2	483.2	493.2
MCF				
Cyclohexane	25.2 ± 0.4	24.1 ± 0.5	25.1 ± 0.7	23.6 ± 1.0
Trichloroethylene	61.3 ± 0.3	59.8 ± 0.5	60.6 ± 0.5	59.8 ± 0.8
Tetrachloroethylene	37.8 ± 0.4	36.4 ± 0.7	36.3 ± 0.6	36.4 ± 0.7
Benzene	67.5 ± 0.2	65.5 ± 0.4	64.8 ± 0.4	64.3 ± 0.7
Toluene	57.4 ± 0.1	56.2 ± 0.2	55.7 ± 0.3	55.4 ± 0.2
0.5 wt% Ni/MCF				
Cyclohexane	28.2 ± 1.0	28.2 ± 0.8	27.7 ± 1.0	27.3 ± 1.2
Trichloroethylene	75.0 ± 0.4	74.4 ± 0.9	74.1 ± 0.4	73.9 ± 0.6
Tetrachloroethylene	42.6 ± 0.8	42.4 ± 0.4	42.3 ± 1.1	41.4 ± 1.2
Benzene	79.9 ± 0.4	78.1 ± 0.6	77.4 ± 1.0	76.2 ± 1.1
Toluene	67.6 ± 0.2	66.3 ± 0.6	65.9 ± 0.7	64.9 ± 0.2
1.0 wt% Ni/MCF				
Cyclohexane	26.0 ± 0.6	25.6 ± 1.0	24.8 ± 0.6	24.6 ± 1.4
Trichloroethylene	69.4 ± 0.6	69.1 ± 1.1	67.2 ± 0.5	66.0 ± 1.1
Tetrachloroethylene	38.4 ± 0.5	38.4 ± 0.3	36.8 ± 0.6	35.8 ± 1.8
Benzene	78.0 ± 0.4	76.9 ± 0.2	74.2 ± 0.3	72.7 ± 0.8
Toluene	66.7 ± 0.5	65.8 ± 0.2	64.2 ± 0.2	63.4 ± 0.1
2.0 wt% Ni/MCF				
Cyclohexane	26.6 ± 0.3	25.6 ± 0.3	24.2 ± 0.4	23.8 ± 0.5
Trichloroethylene	62.9 ± 0.4	62.4 ± 0.6	60.5 ± 0.8	59.4 ± 0.4
Tetrachloroethylene	39.2 ± 0.3	37.7 ± 0.6	36.3 ± 0.5	35.7 ± 0.6
Benzene	67.9 ± 0.2	67.4 ± 0.3	65.4 ± 0.7	63.7 ± 0.9
Toluene	57.9 ± 0.8	57.0 ± 0.7	56.3 ± 0.3	55.1 ± 0.3

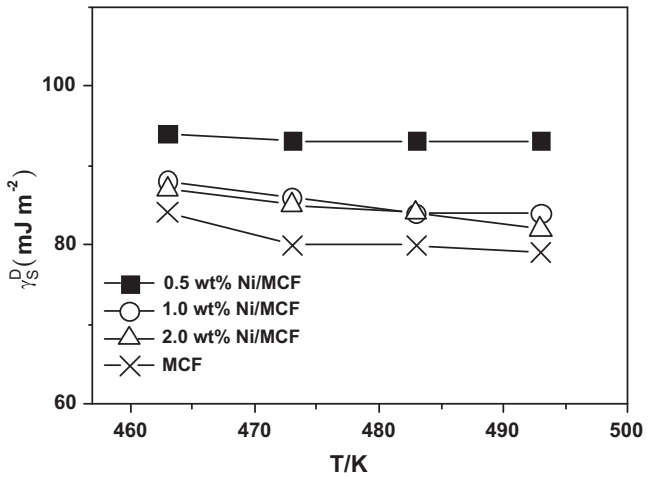

Fig. 7. Dispersive interaction, γ_S^D, of MCF and Ni/MCF samples as a function of temperature.

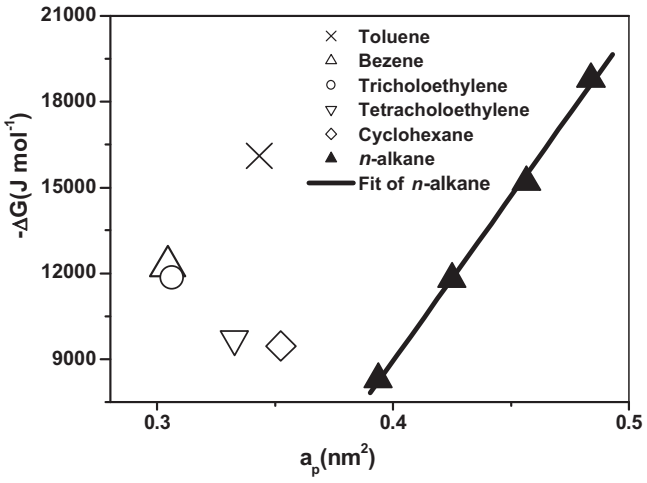

Fig. 8. Specific interaction parameter based on a_p, over 0.5 wt% Ni/MCF at 473.2 K.

other is the Ni species which has electron interaction with aromatic ring [12]. Compared with MCF, the specific interaction with aromatic hydrocarbon on 0.5 wt% Ni/MCF is increased about 20% much greater than the dispersive interaction which is strengthened about 10%, indicating nickel species possess extra specific interaction with aromatic structure.

The effect of Ni particles size on the special interaction of benzene is shown in Fig. 9. The specific interaction for benzene decreases with Ni loading increment, suggesting the main influence is not from the amount of metal modifying sites but from the formed structure of the adsorption centers. For the effect of the metal particle size, highly dispersive Ni species with small particles have the strong specific interaction with benzene in Fig. 9. When Ni species begin to aggregate with metal loading increment, the electron interaction weakens greatly. Further analysis of the error in Table 4 shows the specific interaction with aromatics structure significantly different on the samples of Ni/MCF. This phenomenon indicates the specific interaction of benzene is largely influenced by metal modifying form of the particle size. Small metal particle possesses a great many of the coordinately unsaturated surface atoms, which can interact with aromatic ring strongly [2]. With Ni loading increment, large metal particles form and coordinately unsaturated

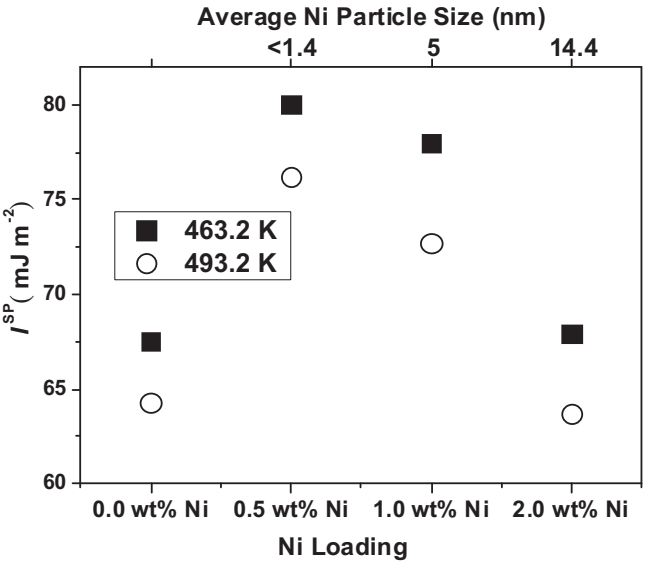

Fig. 9. Dependence of I^{sp} (mJ/m^2) on MCF samples with different Ni loading for benzene at different temperature: 463.2 K (■) and 493.2 K (○).

sites decrease greatly [35], which results in the weak promotion of the specific interaction.

According to the literatures [2,3,35,36], small metal particle with coordinately unsaturated metal atoms can contribute to the catalytic activity in the reaction. Iglesia [35] and Verykios [36] found that the coordinately unsaturated Rh surface atoms prevalent in smaller clusters activate C—H bonds more effectively than the larger one. As for Ni, similar result was proved in hydrogenation of benzene that high turnover frequency (TOF) of benzene occurs over Al_2O_3 loaded with ca. 2 nm Ni particles [2]. The main contribution from small metal particle is the occurrence of coordinately unsaturated metal sites such as the kinks, steps, and corners [35,36], on which aromatic hydrocarbon can be interacted strongly [2,3]. Therefore, the specific interaction, especially electron interaction, shows great increase due to the large existence of coordinately unsaturated sites in the small metal nanoparticles.

4. Conclusions

Inverse gas chromatography at infinite dilution is successfully applied in evaluation of the surface property of MCF loaded with different sized Ni nanoparticles (≤27.4 nm). The adsorption free energy, adsorption enthalpy, dispersive interaction and specific interaction are readily obtained on MCF and Ni/MCF. High adsorption free energy and adsorption enthalpy of aromatic probes was found on 1.0 wt% Ni/MCF with average particle size of ca. 5.0 nm. Strong dispersive and specific interaction especially for aromatic probes was observed on 0.5 wt% Ni/MCF with highly dispersed metal species. It was indicated that Ni/MCF with high metal dispersion possesses the specific surface property of strong electron interaction with aromatics structure due to the large occurrence of coordinately unsaturated metal sites.

Acknowledgments

This work was supported by the National Natural Science Foundation of China (J1103304, 61177021 and 21003024), Fudan's Undergraduate Research Opportunities Program (FDUROP), Fudan's Research Foundation (20520133031) and Shanghai Science and Technology Committee (12DZ2275100).

References

[1] C. Ratanatawanate, M. Macias, B.W.L. Jang, Ind. Eng. Chem. Res. 44 (2005) 9868.
[2] R. Molina, G. Poncelet, J. Catal. 199 (2001) 162.
[3] P.M. Mortensen, J.D. Grunwaldt, P.A. Jensen, A.D. Jensen, ACS Catal. 3 (2013) 1774.
[4] P. Schmidt-Winkel, W.W. Lukens, P.D. Yang, D.I. Margolese, J.S. Lettow, J.Y. Ying, G.D. Stucky, Chem. Mater. 12 (2000) 686.
[5] P. Schmidt-Winkel, W.W. Lukens, D.Y. Zhao, P.D. Yang, B.F. Chmelka, G.D. Stucky, J. Am. Chem. Soc. 121 (1999) 254.
[6] Y.M. Liu, J. Xu, L.C. Wang, Y. Cao, H.Y. He, K.N. Fan, Catal. Lett. 125 (2008) 62.
[7] A. Voelkel, B. Strzemiecka, K. Adamska, K. Milczewska, J. Chromatogr. A 1216 (2009) 1551.
[8] O. Pfohl, R. Dohrn, Fluid Phase Equilib. 217 (2004) 189.
[9] V.I. Bondar, B.D. Freeman, Y.P. Yampolskii, Macromolecules 32 (1999) 6163.
[10] Z.Y. Alsaigh, Int. J. Polym. Anal. Charact. 3 (1997) 249.
[11] M.P. Elizalde-Gonzalez, R. Ruiz-Palma, J. Chromatogr. A 845 (1999) 373.
[12] X.L. Zhang, L.P. Qian, P. Xu, H.Y. He, Q.G. Du, Chem. Eng. J. 137 (2008) 579.
[13] E. Diaz, S. Ordonez, A. Vega, J. Coca, Microporous Mesoporous Mater. 83 (2005) 292.
[14] E. Diaz, S. Ordonez, A. Vega, J. Coca, Microporous Mesoporous Mater. 77 (2005) 245.
[15] C. Bilgic, F. Tumsek, J. Chromatogr. A 1162 (2007) 83.
[16] L.P. Qian, Y. Ren, T.Y. Liu, D.F. Pan, H.T. Wang, G.P. Chen, Chem. Eng. J. 213 (2012) 186.
[17] S.K. Milonjic, Colloids Surf. A 149 (1999) 461.
[18] E. Diaz, S. Ordonez, A. Vega, J. Coca, Microporous Mesoporous Mater. 70 (2004) 109.

[19] X.L. Zhang, L.P. Qian, H.T. Wang, W. Zhong, Q.G. Du, Sep. Purif. Technol. 63 (2008) 434.
[20] N.A. Katsanos, D. Gavril, J. Kapolos, G. Karaiskakis, J. Colloid Interface Sci. 270 (2004) 455.
[21] N.A. Katsanos, R. Thede, F. Roubani-Kalantzopoulou, J. Chromatogr. A 795 (1998) 133.
[22] N.A. Katsanos, N. Bakaoukas, A. Koliadima, G. Karaiskakis, A. Jannussis, J. Phys. Chem. B 109 (2005) 11240.
[23] J. Xie, Q. Zhang, K.T. Chuang, J. Catal. 191 (2000) 86.
[24] J.H. de Boer, The Dynamical Character of Adsorption, Oxford University Press, London, 1953.
[25] G.M. Dorris, D.G. Gray, J. Colloid Interface Sci. 77 (1980) 353.
[26] A. van Asten, N. van Veenendaal, S. Koster, J. Chromatogr. A 888 (2000) 175.
[27] S. Therdthianwong, A. Therdthianwong, C. Siangchin, S. Yongprapat, Int. J. Hydrogen Energy 33 (2008) 991.
[28] D.Y. Zhao, J.L. Feng, Q.S. Huo, N. Melosh, G.H. Fredrickson, B.F. Chmelka, G.D. Stucky, Science 279 (1998) 548.
[29] F. Kleitz, S.H. Choi, R. Ryoo, Chem. Commun. (2003) 2136.
[30] P. Mukhopadhyay, H.P. Schreiber, Macromolecules 26 (1993) 6391.
[31] R.Y. Qin, H.P. Schreiber, Langmuir 10 (1994) 4153.
[32] H.Y. Wang, C.B. Zhang, H. He, L. Wang, J. Environ. Sci. 24 (2012) 473.
[33] L. Shi, Y. Zou, H.Y. He, Chem. Lett. 11 (2001) 1164.
[34] E. Diaz, S. Ordonez, A. Vega, J. Coca, J. Chromatogr. A 1049 (2004) 139.
[35] J. Wei, E. Iglesia, J. Catal. 225 (2004) 116.
[36] Z.L. Zhang, V.A. Tsipouriari, A.M. Efstathiou, X.E. Verykios, J. Catal. 158 (1996) 51.